The Atmospheric Response to Projected Terrestrial Snow Changes in the Late Twenty-First Century

MICHAEL A. ALEXANDER

NOAA/Earth System Research Laboratory, Boulder, Colorado*

ROBERT TOMAS, CLARA DESER, AND DAVID M. LAWRENCE

National Center for Atmospheric Research, Boulder, Colorado

(Manuscript received 18 June 2010, in final form 3 August 2010)

ABSTRACT

Two atmospheric general circulation model experiments are conducted with specified terrestrial snow conditions representative of 1980–99 and 2080–99. The snow states are obtained from twentieth-century and twenty-first-century coupled climate model integrations under increasing greenhouse gas concentrations. Sea surface temperatures, sea ice, and greenhouse gas concentrations are set to 1980–99 values in both atmospheric model experiments to isolate the effect of the snow changes. The reduction in snow cover in the twenty-first century relative to the twentieth century increases the solar radiation absorbed by the surface, and it enhances the upward longwave radiation and latent and sensible fluxes that warm the overlying atmosphere. The maximum twenty-first-century minus twentieth-century surface air temperature (SAT) differences are relatively small (<3°C) compared with those due to Arctic sea ice changes (~10°C). However, they are continental in scale and are largest in fall and spring, when they make a significant contribution to the overall warming over Eurasia and North America in the twenty-first century. The circulation response to the snow changes, while of modest amplitude, involves multiple components, including a local low-level trough, remote Rossby wave trains, an annular pattern that is strongest in the stratosphere, and a hemispheric increase in geopotential height.

1. Introduction

Terrestrial snow cover (SC) can influence the atmosphere via surface heat and radiative fluxes, as it is a good insulator and has both high albedo and thermal emissivity. For example, changes in snow cover during winter alter the surface fluxes, thereby changing the lower-tropospheric temperature (e.g., Walsh et al. 1982; Vavrus 2007). In addition to this local effect, snow cover also generates a remote response that differs depending on the dynamical processes involved. Changes in the Northern Hemisphere annular mode (NAM; Thompson and Wallace 2000) have been linked to the distribution of snow over Siberia via vertically propagating Rossby waves that break in the stratosphere and whose energy subsequently propagates back down into the troposphere (Saito et al. 2001; Gong et al. 2003; Cohen et al. 2007; Fletcher et al. 2009). In contrast to this zonal response, snow cover can also affect storm tracks and horizontal Rossby wave propagation, creating alternating highs and lows (Walland and Simmonds 1996; Vavrus 2007; Orsolini and Kvamstø 2009; Sobolowski et al. 2010). Model projections of climate forced by increased greenhouse gases (GHGs) show a number of changes, including globally averaged warming, a more vigorous hydrological cycle, and an overall reduction in sea ice and snow cover (e.g., Solomon et al. 2007). Changes in the cryosphere, however, do not just passively respond to anthropogenic forcing but also feed back on the climate system. To isolate the role of decreasing Arctic sea ice in climate change, Deser et al. (2010) specified the projected sea ice changes in the late twenty-first century in an atmospheric

* The National Center for Atmospheric Research is sponsored by the National Science Foundation.

Corresponding author address: Michael Alexander, NOAA/Earth System Research Laboratory, R/PSD1, 325 Broadway, Boulder, CO 80305.
E-mail: michael.alexander@noaa.gov

DOI: 10.1175/2010JCLI3899.1

general circulation model (AGCM) while the SST and GHGs were set to their twentieth-century values. In this complementary study, we use a similar experiment design to investigate the seasonal response to projected snow cover changes.

2. Model experiments

To address the climatic effects of projected changes in terrestrial snow cover, we have conducted two experiments with the National Center for Atmospheric Research (NCAR) Community Atmosphere Model, version 3 (CAM3), coupled to the Community Land Model, version 3 (CLM3), where the sea ice and sea surface temperature (SST) are specified. The ''control'' experiment consists of a 60-yr integration with a specified repeating seasonal cycle of land snow fractional coverage, depth, and water content based on the average over 1980–99, obtained from the seven-member ensemble mean of the Community Climate System Model, version 3 (CCSM3) ''twentieth century'' simulations, which includes ocean and sea ice models in addition to CAM3 and CLM3. The twentieth-century simulations were forced with observed estimates of time-varying atmospheric chemical composition (greenhouse gases, ozone, sulfate, and volcanic aerosols) and solar output as described in Meehl et al. (2006). The ''perturbation'' experiment consists of a 60-yr integration with a repeating seasonal cycle of terrestrial snow fractional coverage, depth, and water content for the period 2080–99, taken from the eight-member ensemble mean of twenty-first-century CCSM3 simulations under the Special Report on Emissions Scenarios (SRES) A1B greenhouse-gas-forcing scenario. In both simulations, the SSTs and sea ice are set to those in the control experiment to isolate the direct effect of the terrestrial snow changes. The response is obtained from the difference between the 60-yr averages of the perturbation and control integrations; the statistical significance of the response is evaluated using a two-sided t test where each year is treated as an independent sample.

CAM3 (Collins et al. 2006) and the CLM3 (Oleson et al. 2004) have a horizontal resolution of ~1.4° latitude and 1.4° longitude (T85). The CLM3 has been modified so that the calculated values of snow depth (SD), fractional coverage, and water content are overwritten. The snow state was interpolated to each model time step using monthly ensemble-averaged values from the coupled CCSM3 simulations. After determining that shallow overwritten snow depths were having unrealistically large effects on the surface heat fluxes, all values less than 2 cm were set to zero.

3. Results

The Northern Hemisphere terrestrial SC fraction and SD averaged over the period 1980–99 and the difference (Δ) between 2080 and 2099 (perturbation) and 1980 and 1999 (control) are shown in Fig. 1 for October–December (OND), January–March (JFM), April–June (AMJ) and July–September (JAS). For the control experiment, snow cover extends to central Asia and the central United States during JFM and retreats to Siberia and northwest Canada by JAS, with maximum snow depth at high latitudes and in the Himalayas and Rockies during the cold seasons. While CCSM3 tends to underestimate (overestimate) the mean SC (SD), its simulated change in snow cover due to increased greenhouse gases is near the middle of the Intergovernmental Panel on Climate Change Fourth Assessment Report (IPCC AR4) model distribution (Frei and Gong 2005). Compared to the control, the perturbation experiment exhibits less snow cover ($\Delta SC < 0$) over the entire Northern Hemisphere in all seasons because of the warmer climate induced by increased GHGs, with the largest reductions on the southern flank of the twentieth-century snow distribution and in the mountains of North America and Eurasia (changes in snow cover were negligible over the entire Southern Hemisphere). While snow depth also decreases over most of the Northern Hemisphere, it increases over portions of Siberia and the Canadian Arctic during the cold seasons, especially in JFM. These increases occur in regions that receive more precipitation and remain sufficiently cold for some of it to fall as snow. The increased moisture is primarily supplied by greater evaporation over the Arctic Ocean in the late twenty-first century and the subsequent advection of the moisture over the adjacent continents (Deser et al. 2010).

The specified snow cover/depth changes alter the seasonal differences in the nonsolar surface heat flux (ΔQ_{sfc})—that is, the sum of the sensible and latent fluxes plus longwave radiation (Fig. 2, top row). The fluxes are mainly upward ($\Delta Q_{sfc} > 0$) where the snow cover is reduced, with values generally <10 W m^{-2}, except for high terrain, where they reach a maximum of ~30 W m^{-2}. While ΔQ_{sfc} roughly scales with ΔSC rather than ΔSD, the fluxes are not as strong as implied by the large decreases in snow cover over the northern portions of Eurasia and North America in OND (also see Fig. 4). Regions with negative ΔQ_{sfc} values adjacent to large positive values—for example, over eastern China and the United States during JFM—partly result from the advection of warmer air from upstream locations, where the snow cover is reduced.

The decrease in snow cover also reduces the surface albedo (not shown), thereby increasing the net shortwave

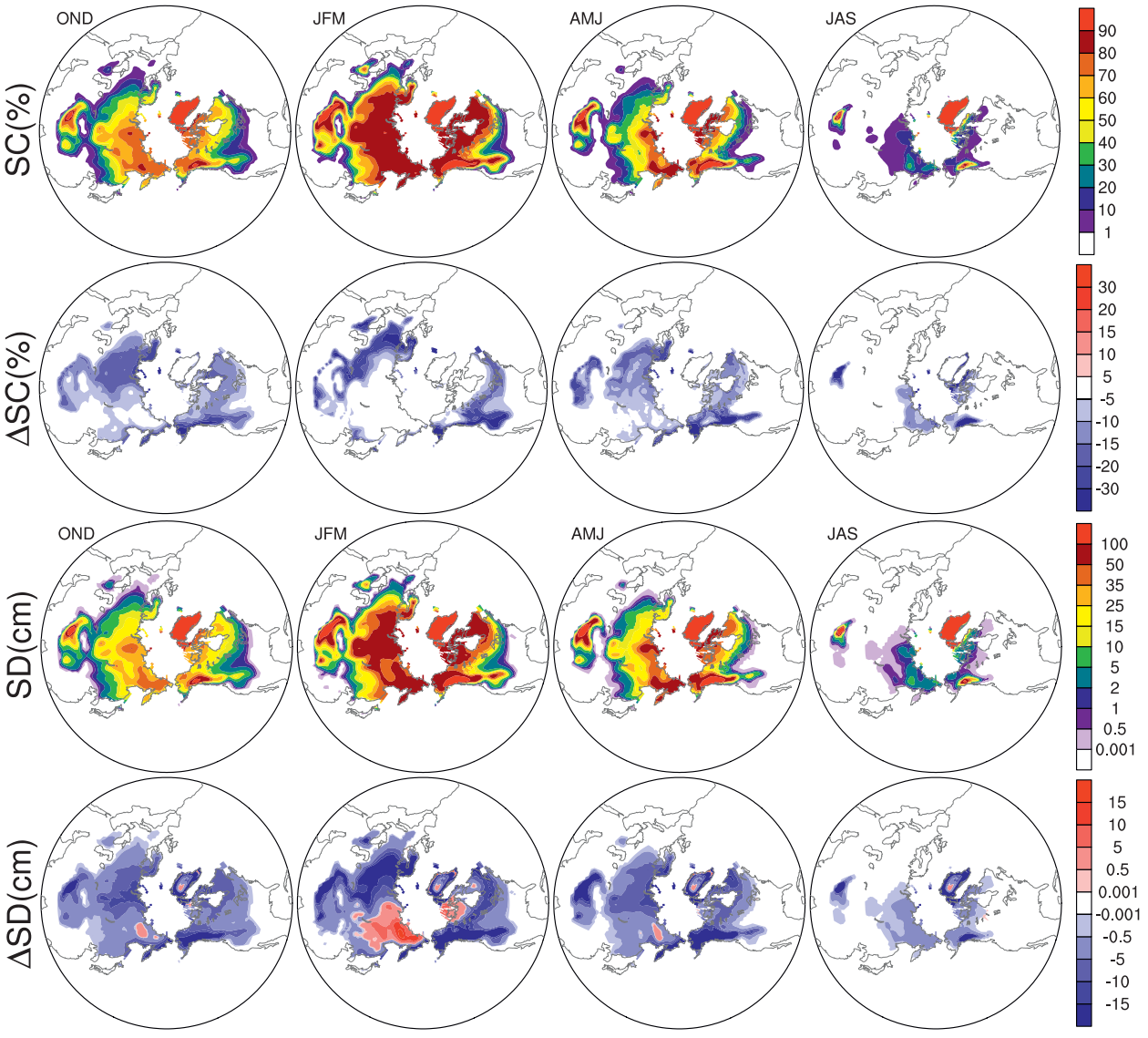

FIG. 1. Seasonal distributions of the average terrestrial SC (%) for (first row) 1980–99 and (second row) 2080–99 − 1980–99 (Δ) and (third and fourth rows) the same distributions for SD (cm) obtained from the CCSM3 and used as boundary conditions for the experiments performed here.

radiation into the surface ($\Delta Q_{sw} > 0$; Fig. 2, middle). However, ΔQ_{sw} is also influenced by the atmospheric response to the reduction in snow, especially changes in low clouds, which strongly reflect sunlight (Fig. 2, bottom). In general, low clouds tend to decrease along and to the south of where the snow cover decreases and increases farther north, although the causes of the low-cloud pattern are unclear. The increase in sunlight at the top of the atmosphere at middle relative to high latitudes, also contributes to the southward enhancement of ΔQ_{sw} in all seasons except summer. The latter two factors enhance and broaden the scale of ΔQ_{sw} in mid-latitudes of Eurasia and North America.

The direct response of the terrestrial surface air temperature differences (ΔSAT) to snow cover changes generally resembles ΔQ_{sfc}, although the former is smoother and of broader scale as the atmosphere advects and diffuses the surface heating (Fig. 3, top). The largest and most extensive ΔSATs occur during OND and AMJ (values of 1.0°–3.0°C), with a relative minimum in JFM and the smallest values in summer (also see Fig. 4). During summer the largest anomalies are located at high latitudes in eastern Asia and western North America, whereas in the other three seasons they are broader in scale and centered farther south and/or located over high elevations.

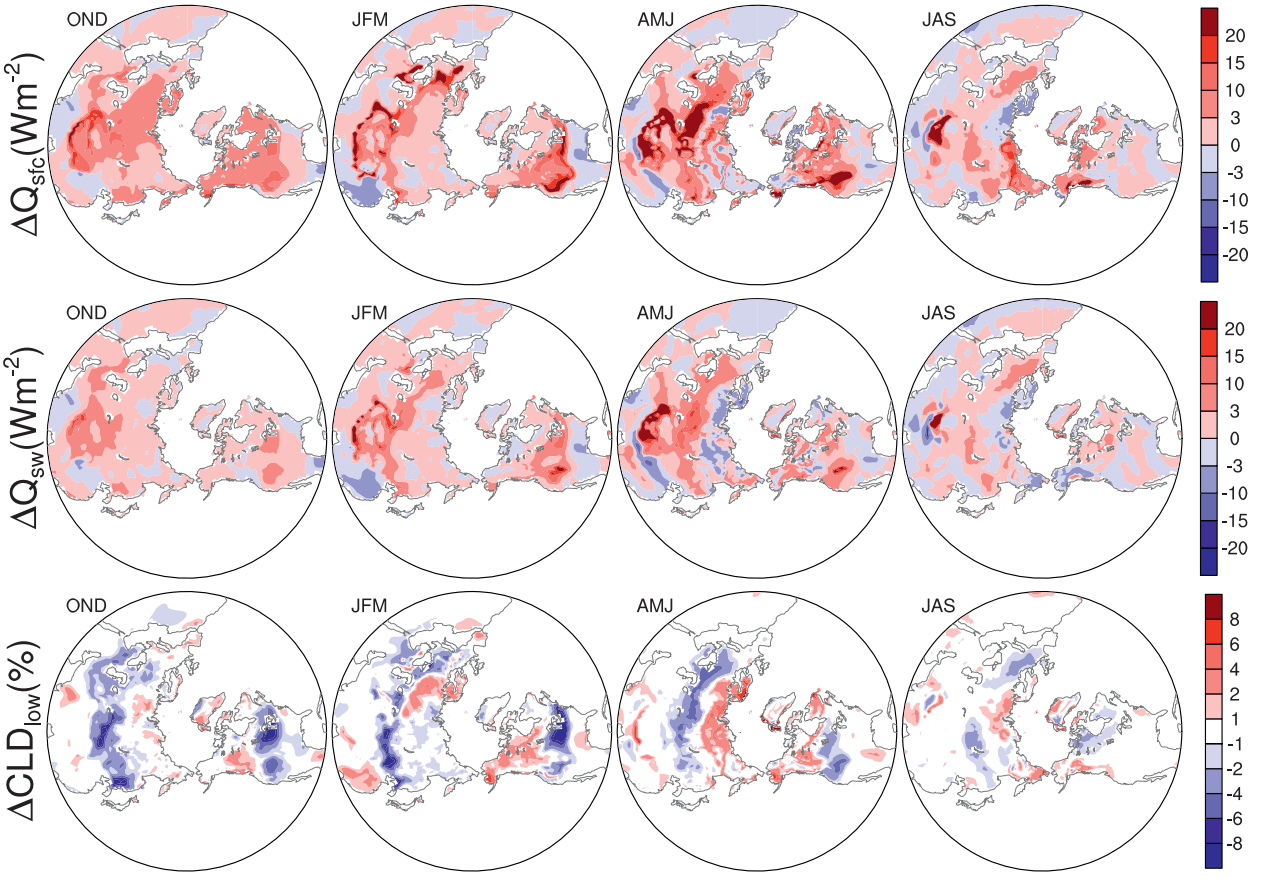

FIG. 2. The difference (Δ) in the seasonal (top) combined sensible, latent, and long wave fluxes at Q_{sfc} (W m^{-2}, positive upward), (middle) Q_{sw} (W m^{-2}, positive downward) and (c) low-level clouds (CLD; %) in response to the SC changes. Nearly all of the $|\Delta Q_{sfc}|$ and $|\Delta Q_{sw}|$ values >3 W m^{-2} are statistically significant at the 95% level as are |ΔCLD| values >2%.

The ΔSAT values from the reduced sea ice experiments of Deser et al. (2010) over the same periods used here are also shown in Fig. 3. While the maximum ΔSAT values are much smaller in response to changes in snow compared to sea ice, the areal coverage of the SAT anomalies is considerably broader than in the sea ice experiments, where they are confined to the rim of the Arctic Ocean. As a result, the changes in snow make a greater contribution to the ΔSAT south of ~55°N in OND and JAS than the changes in sea ice, and they are the dominant cryospheric forcing of ΔSAT over the Northern Hemisphere continents as a whole in AMJ and JAS. The changes in snow make an appreciable contribution to the overall GHG-induced warming over the midlatitudes of Eurasia and North America in fall through spring and over Siberia and Alaska/western Canada in summer, accounting for 10%–30% of the continental-scale warming but exceeding 70% in some regions, when compared to ΔSAT in the full CCSM3 experiments (not shown).

The monthly evolution of ΔSC, ΔSAT, and the top layer soil temperature (ΔT_{soil}) averaged over Eurasia and North America north of 30°N is shown in Fig. 4 (top). For both regions, ΔSAT generally tracks −ΔSC (*y* axis reversed), where both exhibit maxima in fall and spring, with a relative minimum during winter and an absolute minimum during late summer. Unlike ΔSAT, ΔT_{soil} exhibits a strong annual cycle, where ΔT_{soil} is negative in winter and positive in summer. This variation in ΔT_{soil} likely results from the insulating properties of snow; that is, less snow in the twenty-first century allows for the soil to cool more strongly in winter and warm more in summer (Lawrence and Slater 2010).

The surface heat flux is balanced by Q_{sw} and the flux into the ground (Q_{gr}; $Q_{sfc} = Q_{sw} - Q_{gr}$), defined as the flux through a thin interfacial layer into the top full layer of the CLM, which contains snow and/or soil. While ΔQ_{sfc} also exhibits a semiannual cycle over Eurasia and North America, the maxima are much larger in spring then than in fall (Fig. 4, bottom). The spring maxima result from a combination of enhanced ΔQ_{sw} and ΔQ_{gr}, while the flux from the ground helps to maintain positive ΔSAT values in winter.

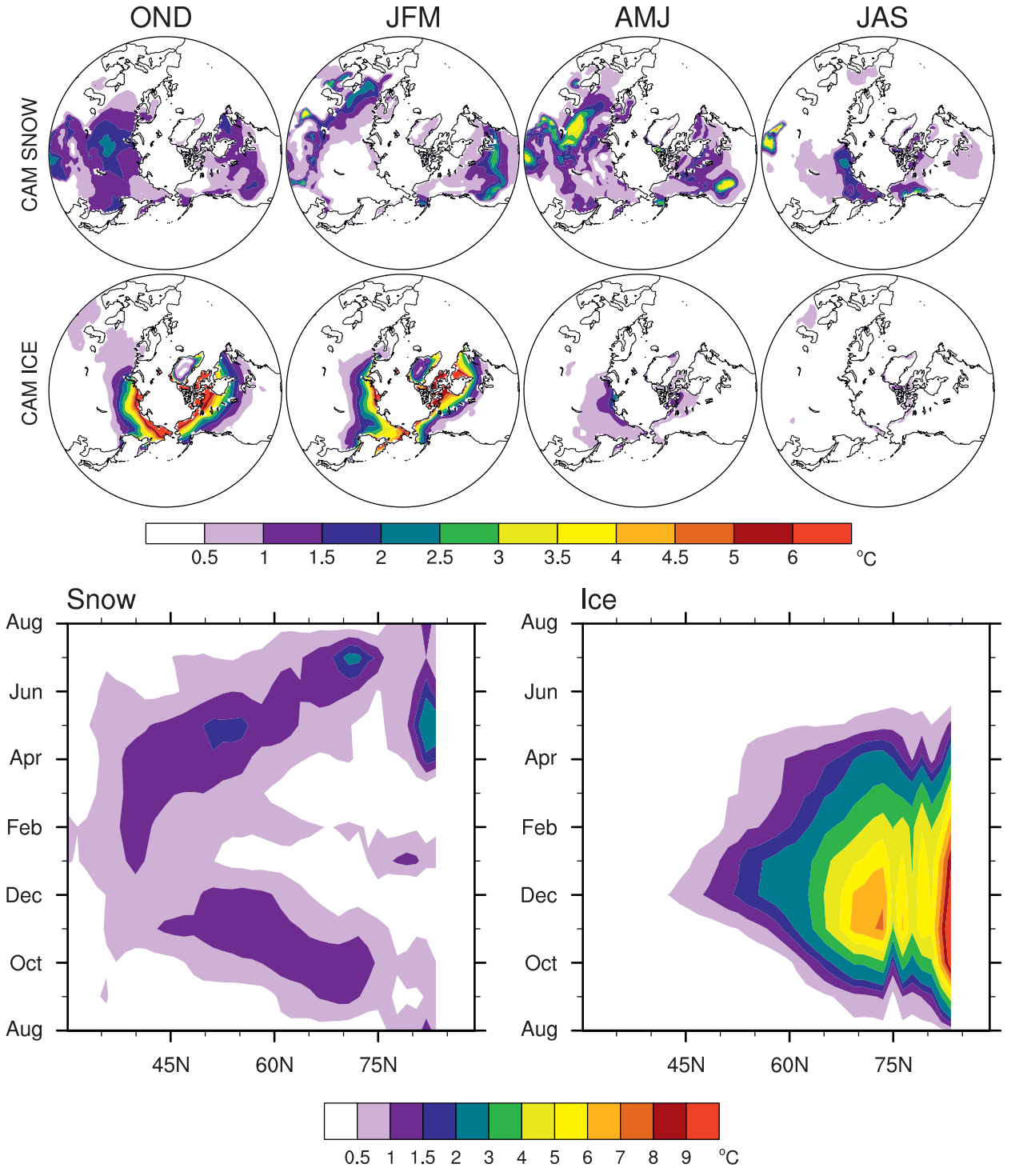

FIG. 3. The ΔSAT (°C) over land in the CAM–CLM (top) SC experiments performed here and (middle) CAM sea ice experiments (see Deser et al. 2010). All of the ΔSAT values >1.0°C and most values >0.5°C are statistically significant at the 95% level. (bottom) Hovmöller diagrams of ΔSAT averaged over land as a function of latitude and calendar month in the (left) SC and (right) sea ice experiments.

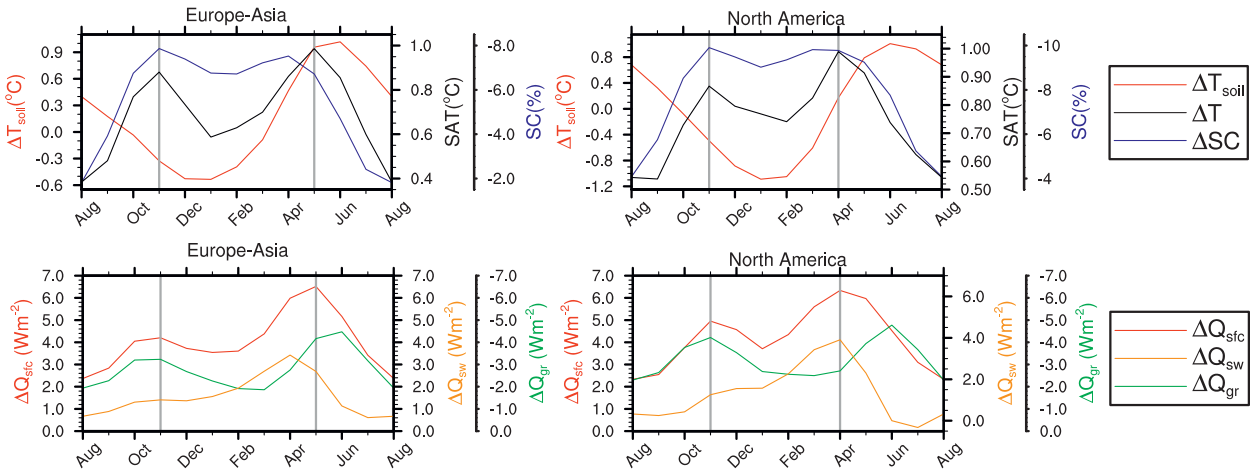

FIG. 4. Seasonal cycle of (top) ΔSC (%; blue line, scale inverted), and ΔSAT (°C; black line) and ΔT_{soil} (°C, red line); (bottom) ΔQ_{sfc}, (W m^{-2}, positive upward, red line), ΔQ_{sw} (W m^{-2}, positive downward, orange line), and ΔQ_{gr} (W m^{-2}, positive downward, green line) averaged over Eurasia and North America north of 30°N. The original raw data for all variables have been smoothed in time with a 1-2-1 filter.

The vertical structure of the atmospheric temperature changes (ΔT) during November and May, the months of maximum or near-maximum ΔSAT (Fig. 4 top), over Eurasia and North America are shown in Fig. 5. In both regions the response is considerably shallower during November, when it is confined below ~700 hPa, compared to May, when the response extends through the troposphere and exceeds 0.2°C up to 300 hPa. The shallow ΔT maximum in November may result from the greater vertical stability in the boundary layer during fall and winter, which limits the vertical penetration of the air warmed by the surface heating. In contrast, the deeper and more uniform ΔT profile in May results from convective heat release and an elevated heat source from melting snow over the Himalayan Plateau and the Rocky Mountains in

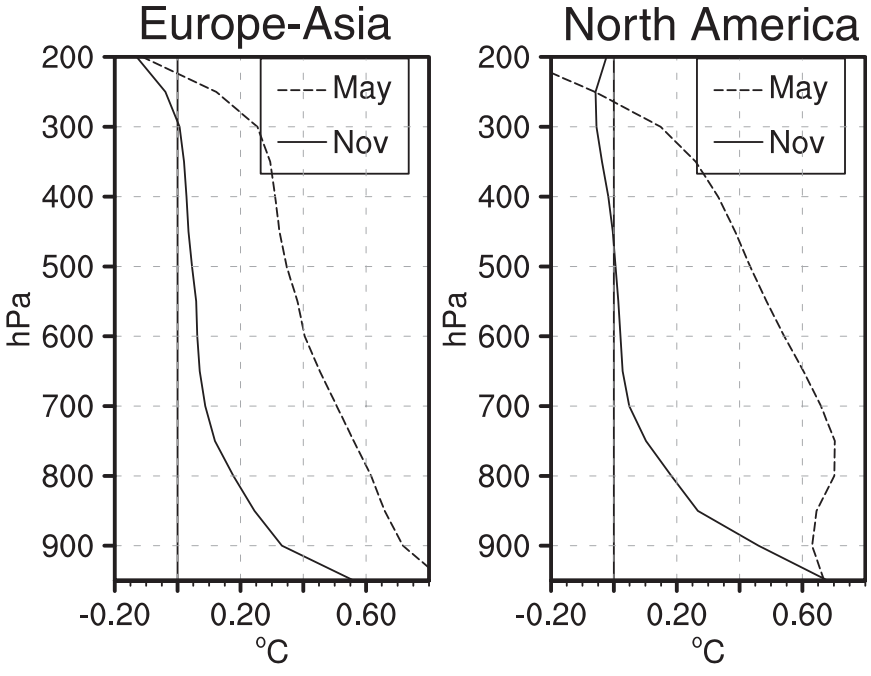

FIG. 5. Vertical profiles of ΔT (°C) during November (solid line) and May (dashed line) over Eurasia and North America. Values below the surface are treated as missing.

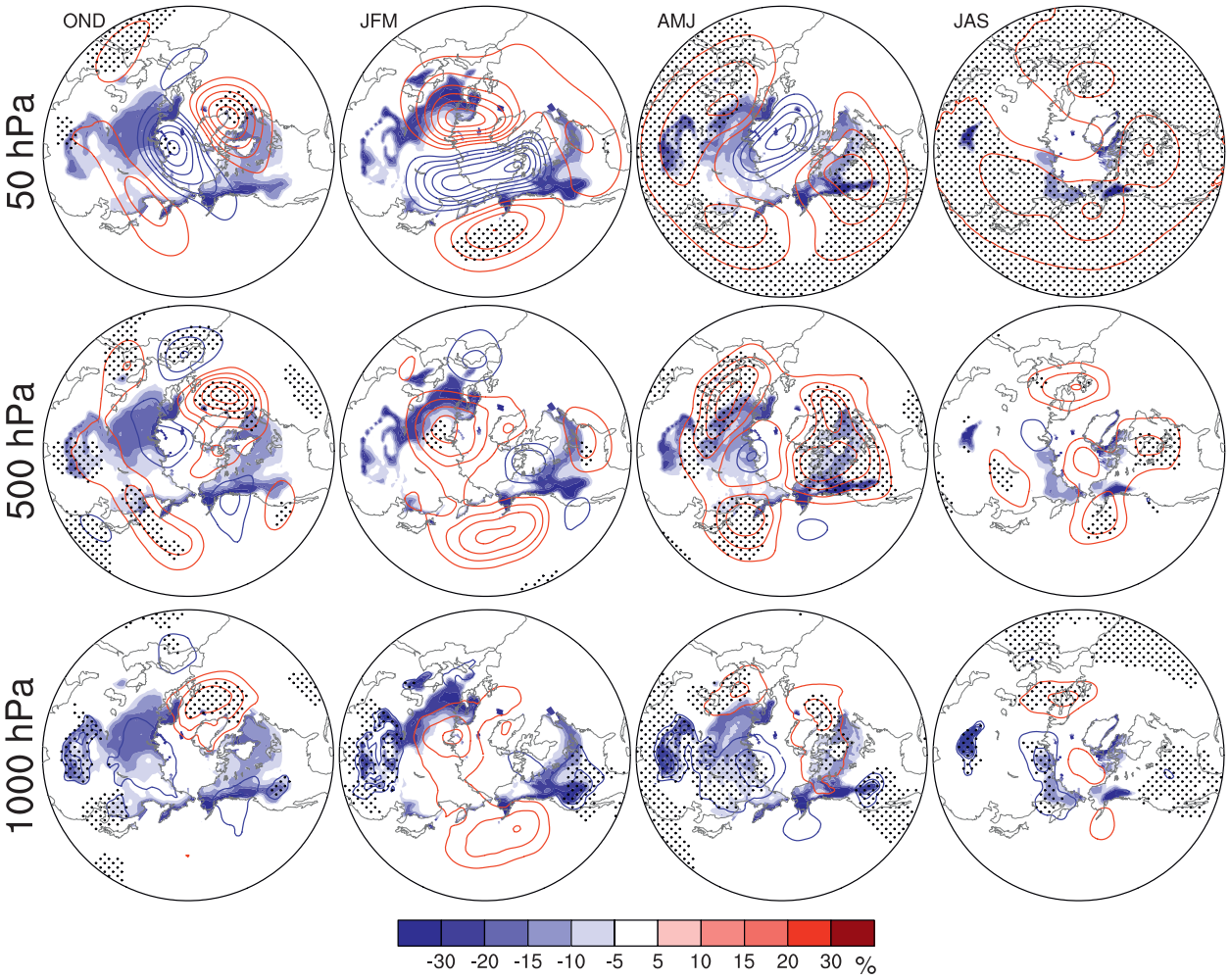

FIG. 6. The Δz response at (bottom) 1000, (middle) 500, and (top) 50 hPa. The contour interval is 5 m with positive (negative) values in red (blue), and the zero contour is omitted. Stippling indicates values that exceed the 95% confidence based on a two-sided Student's *t* test; color shading denotes ΔSC (%).

spring, both of which warm the free troposphere (not shown).

The differences between the twenty-first-century and twentieth-century geopotential height (Δz) at 50, 500, and 1000 hPa are shown for the four seasons in Fig. 6. While the response is of modest amplitude—for example, the maximum Δz values are ~25 m at 500 hPa—they are comparable in magnitude to those in the sea ice experiment (Deser et al. 2010), and many of the features are statistically significant, particularly in spring and fall and at 50 hPa in summer. The response exhibits both relatively small-scale local features and wavelike patterns, along with zonal or nearly hemispheric features. Over most of the Northern Hemisphere continents, the 1000-hPa anomalies indicate a trough where the snow cover is reduced. The remote signal is generally equivalent barotropic through the troposphere (the response at 200 hPa, not shown, has a similar pattern but slightly larger amplitude compared with the anomalies at 500 hPa). The wavelike features, are most prominent at 500 hPa during OND, while a wave 3 pattern is readily apparent from 500 to 50 hPa in AMJ. The stratospheric signal (50 hPa) consists of a low at the pole ringed by higher heights in midlatitudes with two centers in OND and JFM, three centers in AMJ, and a nearly zonal pattern in JAS. Superimposed on these signals is a hemispheric increase in heights due to the general warming of the troposphere, which is most apparent at upper levels during spring and summer.

4. Discussion and conclusions

AGCM simulations were conducted with repeating terrestrial snow cover conditions representative of 1980–99

and 2080–99, with the latter obtained from coupled model simulations using the SRES A1B greenhouse gas scenario. The reduction in snow cover in the twenty-first century relative to the twentieth century increases the solar radiation absorbed by the surface and the upward longwave radiation and latent and sensible heat fluxes, which in turn warm the overlying atmosphere. Decreasing the amount of insulating snow cover increases the heat lost from the ground, resulting in colder soil temperatures but warmer air temperatures during winter. While the maximum ΔSAT due to snow cover changes is much smaller than that due to sea ice changes, the former are broader in scale and more prominent in fall and spring than the sea ice generated ΔSAT. In addition, the SAT response found here may be relatively low, since models that underestimate the present-day snow cover, such as the CCSM, also underestimate the climate sensitivity to snow cover change (Levis et al. 2007).

The atmospheric response to the terrestrial snow changes, while of modest amplitude, appears to involve multiple factors, including a near-surface low over the heating, consistent with the direct response to near-surface thermal forcing in midlatitudes (Hoskins and Karoly 1981; Deser et al. 2007); a remote equivalent barotropic response, which may result from storm-track changes and the horizontal propagation of Rossby wave energy (Honda et al. 1999; Clark and Serreze 2000; Sobolowski et al. 2010); the vertical propagation of energy via Rossby waves creating large-scale patterns in the stratosphere (Cohen et al. 2007), as only long waves are able to penetrate the tropopause (e.g., Holton 2004); and an overall increase in heights due to the broad warming of the Northern Hemisphere. The response patterns found here do not resemble the northern annular mode, as found in some previous AGCM simulations forced by anomalous snow cover or sea ice boundary conditions (e.g., see Deser et al. 2010). Finally, the direct response to the snow cover changes shown here may be altered by feedbacks with other components of the climate system.

Acknowledgments. We gratefully acknowledge support from the National Science Foundation's Arctic System Science Program.

REFERENCES

Clark, M. P., and M. C. Serreze, 2000: Effects of variations in East Asian snow cover on modulating atmospheric circulation over the North Pacific Ocean. *J. Climate,* **13,** 3700–3710.

Cohen, J., M. Barlow, P. J. Kushner, and K. Saito, 2007: Stratosphere–troposphere coupling and links with Eurasian land surface variability. *J. Climate,* **20,** 5335–5343.

Collins, W. D., and Coauthors, 2006: The formulation and atmospheric simulation of the Community Atmosphere Model version 3 (CAM3). *J. Climate,* **19,** 2144–2161.

Deser, C., R. A. Tomas, and S. Peng, 2007: The transient atmospheric circulation response to North Atlantic SST and sea ice anomalies. *J. Climate,* **20,** 4751–4767.

——, ——, M. Alexander, and D. Lawrence, 2010: The seasonal atmospheric response to projected Arctic sea ice loss in the late twenty-first century. *J. Climate,* **23,** 333–351.

Fletcher, C. G., S. C. Hardiman, P. J. Kushner, and J. Cohen, 2009: The dynamical response to snow cover perturbations in a large ensemble of atmospheric GCM integrations. *J. Climate,* **22,** 1208–1222.

Frei, A., and G. Gong, 2005: Decadal to century scale trends in North American snow extent in coupled atmosphere-ocean general circulation models. *Geophys. Res. Lett.,* **32,** L18502, doi:10.1029/2005/GL023394.

Gong, G., D. Entekhabi, and J. Cohen, 2003: Modeled Northern Hemisphere winter climate response to realistic Siberian snow anomalies. *J. Climate,* **16,** 3917–3931.

Holton, J. R., 2004: *An Introduction to Dynamic Meteorology*. 4th ed. Academic Press, 535 pp.

Honda, M., K. Yamazaki, H. Nakamura, and K. Takeuchi, 1999: Dynamic and thermodynamic characteristics of the atmospheric response to anomalous sea-ice extent in the Sea of Okhotsk. *J. Climate,* **12,** 3347–3358.

Hoskins, B. J., and D. J. Karoly, 1981: The steady linear response of a spherical atmosphere to thermal and orographic forcing. *J. Atmos. Sci.,* **38,** 1179–1196.

Lawrence, D. M., and A. G. Slater, 2010: The contribution of snow condition trends to future ground climate. *Climate Dyn.,* **34,** 969–981, doi:10.1007/s00382-009-0537-4.

Levis, S., G. B. Bonan, and P. J. Lawrence, 2007: Present-day springtime high-latitude surface albedo as a predictor of simulated climate sensitivity. *Geophys. Res. Lett.,* **34,** L17703, doi:10.1029/2007GL030775.

Meehl, G. A., and Coauthors, 2006: Climate change projections for the twenty-first century and climate change commitment in the CCSM3. *J. Climate,* **19,** 2597–2616.

Oleson, K. W., and Coauthors, 2004: Technical description of the Community Land Model (CLM). NCAR Tech. Note NCAR/TN-461+STR, 173 pp.

Orsolini, Y. J., and N. G. Kvamstø, 2009: Role of Eurasian snow cover in wintertime circulation: Decadal simulations forced with satellite observations. *J. Geophys. Res.,* **114,** D19108, doi:10.1029/2009JD012253.

Saito, K., J. Cohen, and D. Entekhabi, 2001: Evolution of atmospheric response to early-season Eurasian snow cover anomalies. *Mon. Wea. Rev.,* **129,** 2746–2760.

Sobolowski, S., G. Gong, and M. Ting, 2010: Modeled climate state and dynamic responses to anomalous North American snow cover. *J. Climate,* **23,** 785–799.

Solomon, S., D. Qin, M. Manning, M. Marquis, K. Averyt, M. M. B. Tignor, H. L. Miller Jr., and Z. Chen, Eds., 2007: *Climate Change 2007: The Physical Science Basis*. Cambridge University Press, 996 pp.

Thompson, D. W. J., and J. M. Wallace, 2000: Annular modes in the extratropical circulation. Part I: Month-to-month variability. *J. Climate,* **13,** 1000–1016.

Vavrus, S., 2007: The role of terrestrial snow cover in the climate system. *Climate Dyn.,* **29,** 73–88, doi:10.1007/s00382-007-0226-0.

Walland, D. J., and I. Simmonds, 1996: Modeled atmospheric response to changes in Northern Hemisphere snow cover. *Climate Dyn.,* **13,** 25–34, doi:10.1007/s003820050150.

Walsh, J. E., D. R. Tucek, and M. R. Peterson, 1982: Seasonal snow cover and short-term climatic fluctuations over the United States. *Mon. Wea. Rev.,* **110,** 1474–1485.